Journal Pre-proof
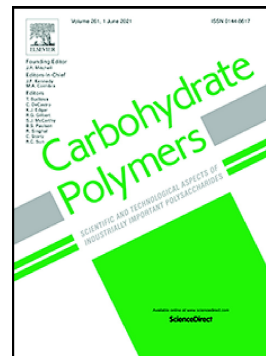
Defensing against oxidative stress in Caenorhabditis elegans of a polysaccharide LFP-05S from Lycii fructus

Fang Zhang, Xia Zhang, Xiaofei Liang, Kanglu Wu, Yan Cao, Tingting Ma, Sheng Guo, Peidong Chen, Sheng Yu, Qinli Ruan, Chunlei Xu, Chunmei Liu, Dawei Qian, Jin-ao Duan

Please cite this article as: F. Zhang, X. Zhang, X. Liang, et al., Defensing against oxidative stress in Caenorhabditis elegans of a polysaccharide LFP-05S from Lycii fructus, *Carbohydrate Polymers* (2021), https://doi.org/10.1016/j.carbpol.2022.119433

This is a PDF file of an article that has undergone enhancements after acceptance, such as the addition of a cover page and metadata, and formatting for readability, but it is not yet the definitive version of record. This version will undergo additional copyediting, typesetting and review before it is published in its final form, but we are providing this version to give early visibility of the article. Please note that, during the production process, errors may be discovered which could affect the content, and all legal disclaimers that apply to the journal pertain.

Defensing against oxidative stress in *Caenorhabditis elegans* of a polysaccharide LFP-05S from *Lycii fructus*

Fang Zhang [a, 1], Xia Zhang [b, 1], Xiaofei Liang [a], Kanglu Wu [c], Yan Cao [a, 2], Tingting Ma [a], Sheng Guo [a], Peidong Chen [a], Sheng Yu [a], Qinli Ruan [c], Chunlei Xu [a], Chunmei Liu [a], Dawei Qian [a] and Jin-ao Duan [a, *]

[a] Jiangsu Collaborative Innovation Center of Chinese Medicinal Resources Industrialization, School of Pharmacy, Nanjing University of Chinese Medicine, Nanjing 210023, PR China;

[b] School of Pharmacy, Key Laboratory of Minority Medicine Modernization, Ministry of Education, Ningxia Medical University, Yinchuan 750021, PR China;

[c] School of Medicine, Nanjing University of Chinese Medicine, Nanjing 210023, PR China;

* Corresponding author at: Jiangsu Collaborative Innovation Center of Chinese Medicinal Resources Industrialization, School of Pharmacy, Nanjing University of Chinese Medicine, Nanjing 210023, PR China. Tel.: +862585811916; Fax: +862585811916; E-mail address: dja@njucm.edu.cn (Jin-ao Duan)

E. mail addresses: fangzhang@njucm.edu.cn (F. Zhang); zhangxia@nxmu.edu.cn (X. Zhang); liangxiaofei@njucm.edu.cn (X. Liang); wukanglu@njucm.edu.cn (K.Wu); yc5347@nyu.edu (Y. Cao); mtt127721@163.com (T. Ma); guosheng@njucm.edu.cn (S. Guo); cpd@njucm.edu.cn (P. Chen); yusheng@njucm.edu.cn (S. Yu); ruanql@njucm.edu.cn (Q. Ruan); xcl127@njucm.edu.cn (C. Xu); liuchunmei@njucm.edu.cn (C. Liu); qiandw@njucm.edu.cn (D. Qian); dja@njucm.edu.cn (J. Duan)

[1] These authors contributed equally to this paper as joint first authors.

[2] Present address: School of Global Public Health, New York University, New York, NY 10003, the United States.

ABSTRACT

Oxidative stress is closely associated with the initiation and progression of aging. Considerable interest centers in the potential application of natural polysaccharides in oxidative stress alleviation and senescence delay. Herein, LFP-05S, an acidic heteropolysaccharide from *Lycii fructus,* was purified and structurally characterized based on a combination strategy of molecular weight (MW) distribution, monosaccharide composition, methylation and NMR spectroscopy analysis. The dominant population of LFP-05S was composed of long homogalacturonan (HG) backbone interspersed with alternating sequences of intra-rhamnogalacturonans-I (RG-I) domains and

branched arabinogalactan and arabinan. Orally supplied LFP-05S exhibited defensive modulation in paraquat (PQ)-damaged oxidative stress *Caenorhabditis elegans* by strengthening the internal defense systems. Under normal conditions, LFP-05S extended the lifespan without significant impairment of propagation. Overall, these results suggested LFP-05S and *L. fructus* are worth further exploration as promising redox-based candidates for the prevention and management of aging and related disorders.

Keywords: *Lycii fructus;* polysaccharide; oxidative stress; structure characterization; *Caenorhabditis elegans*

1. Introduction

The concept of aging basically defines a time-dependent process characterized by an escalated recession of physiological functions, during which a series of aberrant chemical and biochemical events accumulate, leading to compromised self-renewal and self-repair abilities of the organism (Dall & Færgeman, 2019). It is worth noting that the molecular pathogenesis of aging is ambiguously sophisticated and remains open to interpretation. Despite the incompletely interpreted mechanisms, accumulating evidence is supporting a positive correlation between aging progression and oxidative stress recruited from the anomalously robust accumulation of reactive species represented by reactive oxygen species (ROS) (Luo et al., 2020). Consequently, neutralizing excessive ROS production has been considered as a main aspect of persuasive preventative or therapeutic strategies targeting at least one crucial event associated with aging, i.e., severe oxidative stress mediated damage. Some studies have revealed that pharmacological modulation of ROS scavenging improves the oxidative homeostasis and delays the onset and progression of aging and related disorders (Santos et al. 2021). However, the currently used chemical synthetic antioxidants were under suspicion to be associated with liver and kidney damage, gastrointestinal adverse reactions, or even carcinogenesis caused during medication (Poljsak, Šuput and Milisav, 2013). Therefore, this calls for development of novel safe and naturally-occurring interventions that target the oxidative stress homeostasis mechanism, with the overarching goal of a healthy longevity.

Polysaccharides are profusely present across the biosphere, and have been shown to regulate a myriad of fundamentally important intercellular and intracellular processes in the development of multicellularity (Hart & Copeland, 2010). To this effect, studies have demonstrated that polysaccharides possess a multifaceted spectrum of pharmacological benefits, including anti-tumor, anti-oxidative, antiaging, anti-thrombotic, immunomodulatory, and gut microbial modulatory effects (Sindhu et al., 2021; Ben, Haddar, Ghazala, Ben, & Boisset, 2017). Importantly,

polysaccharides are easily endured by the human body, and naturally biocompatible with nontoxic characteristics (Imre, García, Puglia, & Vilaplana, 2019). Application of natural sourced polysaccharides as promising ROS scavenger is a rising concern in the defense against a variety of oxidative stress models, which supports the protective or therapeutic potency of polysaccharides (Eder et al., 2021).

Lycii fructus (Goji berry or Wolfberry), the reddish orange fruit of the perennial solanaceous shrubbery *Lycium barbarum* L., has long been appreciated by international cuisine as a super functional food and raised much interests evaluating its nutritive, preventive and therapeutic properties as exemplified by hepatoprotection, immunoregulation, antioxidation, anti-aging, eyesight protection and cancer prevention (Xiao, Deng, Zhou, & Zhang, 2022).

It is increasingly becoming apparent that the predominant ingredient polysaccharides (LFPs) are specifically involved in *L. fructus's* antioxidative capacity. Over the years, interdisciplinary research has been performed to evaluate the antioxidant and antiaging properties of LFPs (Meng, Lv, Sun, Qiao, & Chen, 2020; Zhang et al., 2019). A recent study found that a crude water-extract of LFPs inhibited the production of excessive ROS and reduced Aβ levels in an Alzheimer's disease model of Caenorhabditis elegans (Meng et al., 2022). Nevertheless, there is only a handful of studies on the effect of well-structural characterized LFPs towards aging, particularly on oxidative stress relief or delaying aging progression (Zhou, et al., 2018). Our previous study found that LFP-1, an acidic heteropolysaccharide mainly composed of arabinogalactan (AG) backbone, moderate amount of HG fragments and short RG-1 segments, exhibited trophic and protective properties in chemical oxidant MPP$^+$-induced injury in PC12 cells (Zhang et al., 2020). Based on these findings, we hypothesized that LFPs are promising ROS scavengers, and may be persuasive redox-based candidates for the prevention and management of aging. Therefore, the main aim of this study was to explore the potential of LFPs in oxidative stress alleviation and senescence delay. Specifically, a purified acidic fraction, LFP-05S, was exploited at the organismal level upon a microscopic nonrodent nematode C. elegans, which offers valuable clues to the intricacies of aging and related diseases. Considering that the biological activities of natural polysaccharides are highly dependent upon their chemical fine structures, particular attention was paid to characterization of the structural organization features of LFP-05S by means of molecular weight distribution, linkage analysis and NMR spectroscopy analysis. Results indicated that LFP-05S neutralized the untoward overproduction of ROS, enhanced the stress resistance and improve the lifespan in C. elegans. Collectively, our findings will provide valuable insights for the development of LFP-05S into a novel product from *L. fructus* for the prevention and management of aging and related declines.

2. Materials and Methods

2.1. Materials and reagents

L. fructus was provided by Bairuiyuan Gouqi Co. Ltd. (Yinchuan, China) and was validated by the corresponding author (Dr. Jin-ao Duan) in accordance with the morphological and histological standards of Chinese Pharmacopoeia (2015 version). Voucher specimen was deposited in Jiangsu Collaborative Innovation Center of Chinese Medicinal Resources Industrialization (Voucher No. LF20170711BRY). DEAE-52 cellulose and Sephacryl S-300HR were purchased from Whatman Ltd (Kent, UK) and GE Healthcare Life Sciences (Piscataway, NJ, USA), respectively. Standard monosaccharide references were purchased from National Institute for Food and Drug Control (Beijing, China). Nitric oxide (NO) assay kit was purchased from YiFeiXue Bio Tech (Nanjing, China). All other oxidative stress indictor kits, including malondialdehyche (MDA) assay kit, superoxide dismutase (SOD) assay kit, catalase (CAT) assay kit, glutathione reductase (GR) assay kit, oxidized glutathione disulfide (GSSG) assay kit and reduced glutathione (GSH) assay kit, were purchased from Beyotime Biotech (Shanghai, China). All other chemicals and solvents were of the highest grade available.

2.2. Extraction and purification of LFP-05S

The acidic polysaccharide LFP-05S was extracted and purified from *L. fructus* following a previously described protocol (Zhang et al., 2020), but with subtle modifications. Briefly, the smashed fruits were refluxed with distilled water (twice at 90°C, each for 2 h) after removal of small molecules and lipids. The polysaccharides were then precipitated with ethanol and deproteinated with Sevag reagent. Next, the fractionation of the deproteinized LFPs was realized stepwise on a DEAE-52 cellulose column (either 4.5 cm × 60 cm or 4.5 cm × 80 cm) with a sequential elution of water, and 0.1 M, 0.2 M, 0.3 M, 0.4 M, 0.5 M and 2 M aqueous NaCl based on the diversities of charge characteristics. The acidic eluate corresponding to 0.5 M NaCl was pooled, desalted and further fractionated on a Sephacryl S-300HR gel permeation chromatography column (2 cm × 90 cm), followed by elution with 0.9% NaCl at a flow rate of 0.40 mL/min. Finally, the purified fraction was concentrated, desalted and lyophilized to generate LFP-05S, which was then subjected to structural elucidation and activity evaluation.

2.3. Structural characterization of polysaccharide moiety of LFP-05S

2.3.1. Morphological analysis

Photomicrographs of the morphological features were recorded using a field emission scanning electron microscope (JSM-7800F, JEOL Ltd., Akishima, Tokyo, Japan) in secondary electron mode at an accelerating voltage of 30 kV.

2.3.2. Homogeneity and MW assays

Homogeneity and MW distribution profile was visualized using size-exclusion chromatography-multi-angle laser light-scattering and refractive index (SEC-MALLS-RI) on a DAWN HELEOS-II laser photometer (He-Ne laser, λ=663.7 nm, Wyatt Technology Co., Santa Barbara, CA, USA) coupled to a differential RI detector (Optilab T-rEX, Wyatt Technology Co., Santa Barbara, CA, USA). Separation was performed on a series of tandem SEC columns (Shodex OH-pak SB-805, 804 and 803; Showa Denko K.K., Tokyo, Japan 8.0× 300 mm, 6 μm, Showa Denko K.K., Tokyo, Japan) at 45°C and equilibrated with 0.1 M $NaNO_3$ as mobile phase. For detection, 100 μL of sample dissolved in 0.1 M $NaNO_3$ at 1 mg/mL was loaded and eluted at 0.4 mL/min.

2.3.3. Monosaccharide and uronic acid composition assays

Monosaccharide and uronic acid composition of LBP-05S was simultaneously determined through GC-MS analysis of the corresponding alditol acetates and N-propylaldonamlde acetates derivatives, respectively, after liberation in 2 M TFA at 110 °C for 2 h (Lehrfeld, 1987). Separation was achieved on an Agilent 7000C GC/MS Triple Quad system (Agilent Technologies, Santa Clara, CA, USA) equipped with an Agilent HP5-ms capillary column (30 m × 0.25 mm × 0.25 μm) with a previously described temperature program (Zhang et al., 2020). Identification was inferred by comparison with the in-house built standards of known concentrations.

2.3.4. Glycosidic linkage assays

The glycosidic linkage patterns were comprehensively analyzed based on a combination strategy of identification and quantification of partially methylated alditol acetates (PMAAs) following the protocols described by Pettolino (Pettolino, Walsh, Fincher, & Bacic, 2012) and Sims (Sims, Carnachan, Bell, & Hinkley, 2018)(see details in the supplementary material). The acetylated PMAAs were identified by integrating the peaks of their relative retention times and diagnostic mass fragmentation patterns visualized in GC-MS, followed by comparison with the standard atlas (https://glygen.ccrc.uga.edu/ccrc/specdb/ms/pmaa/pframe.html) and previously verified spectra in literature.

2.3.5. NMR spectroscopic analysis

For NMR studies, 30 mg of LFP-05S sample was deuterium-exchanged three times in 20 mM NaOD prepared in deuterium oxide. Next, an AVANCE AV-600 NMR spectrometer (Bruker AVANCE AV-600, Rheinstetten, Germany) was operated at 600 MHz and 22 °C to collect ^{1}H NMR, ^{13}C NMR and heteronuclear 2D NMR spectra, including [1]H-^{1}H correlation spectroscopy (COSY), total correlation spectroscopy (TOCSY), nuclear overhauser effect spectroscopy

(NOESY), ^{1}H-^{13}C heteronuclear singular quantum correlation (HSQC) and heteronuclear multiple bond correlation (HMBC) spectra with Sodium 3-(Trimethylsilyl) Propionate (TMSP) as internal standard (^{1}H 0.00 ppm; ^{13}C 0.00 ppm), and then processed using MestReNova 6 software (Mestrelab Research, Escondido, USA). Signal assignment was facilitated by the online repository for NMR data (Biological Magnetic Resonance Data Bank, https://BMRB.io, entry IDs: bmse000228 for Galacturonan, bmse000013 and 001006 for Gal, bmse000213 for Ara, bmse000569 for Glc, respectively) and spectra scattered in literature (Agrawal, 1992; Redgwell et al., 2011; Nguyen, Do, Nguyen, Pham, & Nguyen, 2011; Grasdalen, Einar Bakøy, & Larsen, 1988; Oliveira et al., 2017).

2.4. Defensive effect of LFP-05S on PQ-induced oxidative stress in C. elegans

2.4.1. Maintenance and synchronization of C. elegans strains

Bristol strain N2 was used as a wild-type strain, whereas a transgenic strain with enhanced green fluorescence protein GST-4::GFP fusion expression CL2166 (dvIs19[pAF15(gst-4::GFP::NLS)]) was used as an indicator of inner oxidative stress. Both strains and the auxotrophic uracil bacteria *Escherichia coli* strain OP50 were originally provided by Caenorhabditis Genetics Center (University of Minnesota, Minneapolis, MN, USA).

Nematodes were maintained and cultured under standard condition at 20 °C on agar nematode growth media (NGM) coated with lawn of live *E. coli* OP50 solution as nutritional supply. A day prior to the experiment, age-synchronized population of first larval stage (L1) worms were obtained by NaOH and HClO bleaching from gravid hermaphrodites, followed by hatching of the centrifugal purified eggs in M9 buffer overnight. Notably, synchronized population of L4 worms were obtained three days after synchronization of L1 (Duangjan, Rangsinth, Gu, Wink, & Tencomnao, 2019).

2.4.2. Exposure of CL2166 worms to LFP-05S and/or paraquat (PQ)

To assess the protective potential of LFP-05S against intracellular free-superoxide-generator PQ-induced oxidative stress, synchronized L4 CL2166 worms were randomly allocated into five groups based on their treatment with LFP-05S and/or PQ, and then they were transferred into 50 mM 5-Fluoro-2'-Deoxyuridine (FuDR)-containing NGM plates to block progeny. The exposure scheme was shown in Fig. 5A. Briefly, synchronized L4 worms were cultured under monoxenic conditions with different concentrations of LFP-05S (0, 0.5, 1.0 and 2.0 mg/mL^{-1}) in OP50 suspension for 48 h, followed by treatment with of 20 mM PQ for 4 h to mimic pathological features of oxidative stress. Next, worms were again transferred to PQ-free NGM plate with indicated concentrations of LFP-05S and allowed to recover for an additional 48 h. Worms that only suffered plate shift in standard NGM plates were used as the vehicle control.

2.4.3. Survival assay

Survival was assessed at the end time points of the treatment as described in 2.4.2. Notably, each group had ~30 worms per plate for a total of 100−130 individuals per group. Worms that failed to respond upon repeated gentle mechanical prodding were declared dead and removed from the dish (Goya et al., 2020).

2.4.4. Measurement of lipofuscin accumulation

The accumulation of lipofuscin granules, the classical autofluorescent age pigment, was evaluated by imaging and measuring the relative fluorescence intensity of lipofuscin. Briefly, randomly selected worms (about 10 worms per plate) were paralyzed using 10 mM Imidazole hydrochloride, mounted on 2% agar, and imaged captured under an AxioScope A1 fluorescence microscope (Zeiss, Göttingen, Germany). The relative fluorescence was quantified by software ImageJ (https://imagej.nih.gov/ij/).

2.4.5. In situ measurement of intracellular ROS generation

Worms were harvested, collected by centrifugation, reconstituted in M9 solution containing 250 nM of cell-permeable fluorogenic probe 2,′-dichlorodihydrofluorescein-diacetate (H_2DCF-DA), and then incubated at 20°C for 2 h in the dark. After incubation and extensive washing with M9 buffer, photographic images (about 6-8 worms per plate) were recorded and analyzed as described in section 2.4.4 by quantifying the fluorescence intensity of DCF in intact worms.

2.4.6. Biochemical measurement of oxidative stress and antioxidant biomarkers

Worms (~ 5, 000 larvae on one plate, ~ 15,000 larvae per group) were harvested for the endpoint measurement to evaluated the oxidative stress-related physiological status. Commercially available kits were used to determine the levels of NO and MDA (as oxidative damage markers), and the activities and levels of SOD, CAT, GR, GSSG and GSH (as anti-oxidant markers) in accordance with the manufacturer's instructions.

2.5. Longevity assay

2.5.1. Lifespan analysis

Synchronous L4 N_2 worms were transferred onto 3 cm fresh plates (about 30 worms per replicate for a total of 100−130 individuals per group on FuDR supplement NGM plates) dribbled with OP50 suspension containing different concentrations of LFP-05S and cultured at 20°C. For the continuous feeding duration, worms were transferred to a fresh plate with corresponding LFP-05S concentration every day or at a 2-3 day interval depending on the reproduction phase. Survival was scored every day according to the same criterion as in 2.4.3 until all worms died.

2.5.2. Progeny assay

During the reproductive period (approximately days 1–5), original adult nematodes were individually transferred to fresh plates every day and allowed to deposit embryos. One day after plate shift, progeny number (the number of offspring) on the original plates was recorded and used to calculate the mean progeny produced through the consecutive period per adult worm.

2.6. Statistical analyses

All data are presented as mean ± standard error of the mean (SEM) of a minimum of three independent experiments performed in three biological replicates at similar conditions for statistical analysis unless otherwise specified. Graphs and all statistical analyses were performed by GraphPad Prism 8.0.1 for Windows (GraphPad Software, San Diego, CA, USA, www.graphpad.com). One-way analysis of variance (ANOVA; 95% confidence interval), followed by Dunnett's multiple comparison tests were performed to compare more than two data sets. For lifespan assay, the statistical significance was determined by a log-rank (Mantel–Cox) test fit to Kaplan–Meier method.

3. Results and discussion

3.1. Purification, surface morphology, homogeneity and composition of LFP-05S

An acidic fraction LFP-05S was successfully achieved via subsequent purification by ion-exchange and gel filtration chromatography. The classical phenol-sulfuric acid assay estimated the total carbohydrate content was 85.78%. After lyophilization, this fluffy and yellowish fraction exhibited a pronounced interconnected porous network with smooth surface appearance and irregular pore distribution (Fig.1A). On SEC-MALLS-RI, LFP-05S showed a dominant symmetrical polymer population with a weight-average MW of 4.94×10^4 Da and a polydispersity index of 1.095(Fig.1B). LFP-05S was an acidic heteropolysaccharide mainly composed of Rha, Ara, Glc, Gal and GalA at molar ratio of 7.00%: 8.93%: 7.37%: 9.95%: 60.55%, respectively, with minor components of Xyl (1.16%) and Man (2.47%) (Fig.1C). Notably, the percentage of GalA was particularly high, comprising approximately 60% of LFP-05S, which indicated that the HG domain may primarily compose the molecular structure. The substantial amounts of Glc indicated the possible existence of glucan, which may originate from co-extraction or hydrolysis of other cell wall constituents and explained the presence of a minor peak with lower MW following the main peak in RI detection.
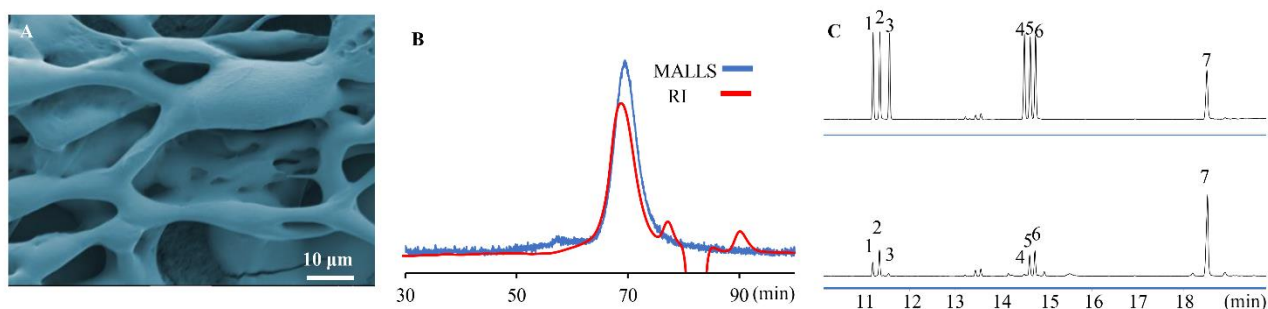
Fig.1. Surface morphology, homogeneity and composition of LFP-05S. (A) Typical micrographic aspect; (B) HPGPC profile on Shodex SB-805 chromatographic columns; (C) GC-MS profile of the acetylated monosaccharides and uronic acids of mixed standards (upper) and LFP-05S (lower). Peaks: (1) Rha, (2) Ara, (3) Xyl, (4) Man, (5) Glc, (6) Gal and (7) GalA.

3.2. Glycosidic linkage position

A panel of 20 acetylated PMAAs were identified based on careful diagnosis of the mass fragments as tabulated in Table 1 (Fig.2 for total ion chromatography of carboxyl-reduced LFP-05S and Fig. S1 for mass spectra of the targeted peaks). Thereinto were eight D-Gal$p$ residues with the most abundant residue being 1,4-linked D-Gal$p$ residue [→4)-Gal$p$-(1→]. Four Ara$f$-based residues, one Xyl$p$ residue, three Glc$p$-based residues and two Rha$p$-based residues were also identified, which provided a good overview of the relative abundance of the potential structural domains.
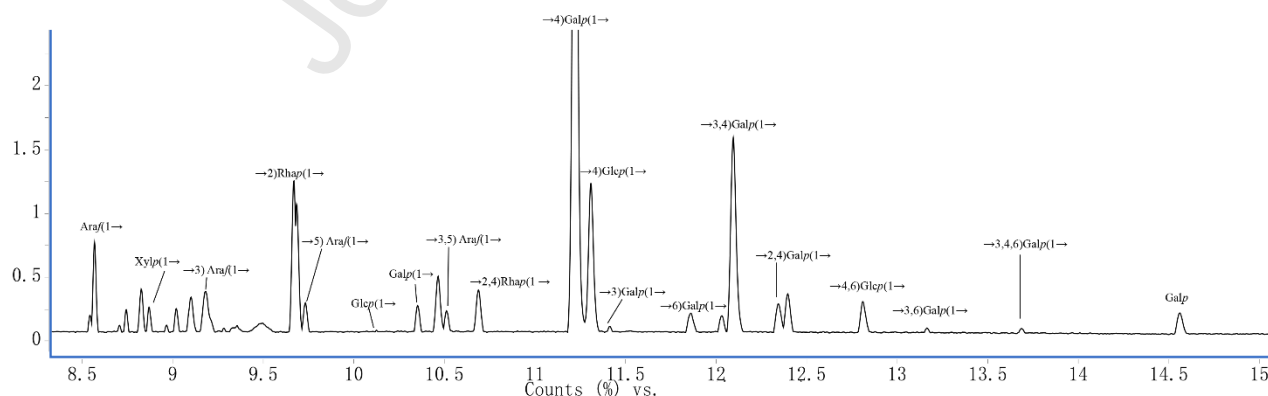

Fig.2. Total ion chromatogram of PMAAs for carboxyl-reduced LFP-05S. Source data are provided in Fig. S1 for the identification of each target peak annotated in the total ion chromatogram, and Fig.S2 for determination of [→4) Gal$p$ (1→] and [→4) Glc$p$ (1→].

Specifically, integrated by the heights of m/z 161:163 and m/z 205:207 of the NaBD$_4$/ NaBD$_4$ reduction in which both methyl esterified and free uronic acids were reduced, ∼ 55% of the Gal$p$-(1→ signal was derived from the reduced Gal$p$A-(1→ residue. Furthermore, 100% of the →4)-Gal$p$-(1→ residues arose from →4-Gal$p$A-(1→ in the parent unreduced LFP-05S, calculated by heights of m/z 233:235 of the NaBD$_4$/ NaBD$_4$ reduction, which was consistent with the high proportions of GalA in the monosaccharide analysis. Likewise, ∼ 85% of the →4)-Gal$p$-(1→ residues were methyl esterified, also calculated by heights of m/z 233:235 of the NaBD$_4$/ NaBH$_4$ reduction, indicating a high percent of methylation modification of Gal$p$A (Fig.S2 for the selected region of the mass spectra for the origin of →4)-Gal$p$-(1→) (Sims et al., 2018). In sharp contrast, Glc$p$A was nonexistent as indicated by the very small percent of the m/z 235 fragment representing the natural abundance of the ^{13}C isotope in the spectrum of →4)-Gal$p$-(1→ derived PMAA after NaBD$_4$/ NaBD$_4$ reduction.

Table 1 Glycosidic linkage composition of carboxyl reduced LFP-05S

Peak	Glycosidic linkages	RT[1]	PMAA	Fragments(m/z)	Mol %*
1	Araf-(1→	8.58	1,4-di-O-Ac-2,3,5-tri-O-Me3 arabinitol	102, 118,129,161	4.51
2	→ 3)-Araf-(1→	9.37	1,3,4-tri-O-Ac-2,5-di-O-Me arabinitol	101, 113, 118,161, 202	3.59
3	→ 5)-Araf-(1→	9.75	1,4,5-tri-O-Ac-2,3-di-O-Me arabinitol	102,118,129,189	1.43
4	→ 3, 5)-Araf-(1→	10.52	1,3,4,5-tri-O-Ac-2-O-Me arabinitol	85, 99, 118, 127,159, 201, 261	1.43
	Total				10.96
5	Xylp-(1→	8.88	1,5-di-O-Ac-2,3,4-tri-O-Me xylitol	102, 118, 131, 161	1.66
	Total				1.66
6	→2)-Rhap-(1→	9.70	1,2,5-tri-O-Ac-6-deoxy-3,4-di-O-Me rhamnitol	131, 190	7.89
7	→2,4)-Rhap-(1→	10.70	1,2,4,5-tetra-O-Ac-6-deoxy-3-O-Me rhamnitol	101, 130, 143, 190, 207	1.60
	Total				9.49
8	Galp-(1→	10.37	1,5-di-O-Ac-2,3,4,6-tetra-O-Me galactitol	102, 118, 129, 145, 161, 205	1.67
9	→3)-Galp-(1→	11.42	1,3,5-tri-O-acetyl-2,4,6-tri-O-methyl galactitol	101,118,129,174,235	0.87
10	→6)-Galp-(1→	11.93	1,5,6-tri-O-acetyl-2,3,4-tri-O-methyl galactitol	99,101,118,129,161,173,233	0.53
11	→3,6)-Galp-(1→	13.18	1,3,5,6-tetra-O-Ac-2,4-di-O-Me galactitol	118, 129, 139, 160, 189, 234	0.91
12	→3,4,6)-Galp- (1→	13.68	1,3,4,5,6-penta-O-Ac-2-O-Me galactitol	118,139,160,333	0.44
13	Galp	14.55	1,2,3,4,5,6-hexa-O-Ac-galactitol	115,128, 145, 157, 170, 187, 217	3.74
	Total				8.16
14	GalpA-(1→	10.37	1,5-di-O-Ac-2,3,4,6-tetra-O-Me galactitol	102, 118, 129, 145, 161, 205	2.04
15	→4)-GalpA-(1→	11.24	1,4,5-tri-O-acetyl-2,3,6-tri-O-methyl galactitol	102, 113, 118, 131, 161, 173, 233	47.90
16	→3,4)-GalpA-(1→	12.10	1,3,4,5-tetra-O-Ac-2,6-di-O-Me galactitol	118, 129, 143, 160, 185	6.40
17	→2,4)-GalpA-(1→	12.37	1,2,4,5-tetra-O-Ac-3,6-di-O-Me galactitol	113, 130, 190, 233	2.35
	Total				58.69
18	Glcp-(1→	10.13	1,5-di-O-Ac-2,3,4,6-tetra-O-Me glucitol	102, 118, 129, 145, 161, 205	1.64
19	→4)-Glcp-(1→	11.32	1,4,5-tri-O-Ac-2,3,6-tri-O-Me glucitol	113, 118, 131, 161, 173, 233	7.42

| 20 | →4,6)-Glcp-(1→ | 12.83 | 1,4,5,6-tetra-O-Ac-2,3-di-O-Me glucitol | 102, 118, 127, 142, 201, 261 | 1.97 |
| | Total | | | | 11.04 |

[1] RT: retention time (min); [2] Ac: acetyl; [3] Me: methyl.

*: average of three individual experiments. Source data are provided in Table S1 for the calculation process of relative abundance (Mol %).

Some of the detected peaks could not be readily assigned because their fragmentation patterns did not correspond to any characterized PMAAs and further hindered the requirements of precise structural characterization. The emergence of these peaks might originate from undermethylation or co-elution of the derivatives from the column although other possibilities remained. Along with the T-Gal or branched Gal glycosyl residues that commonly present in heteropolysaccharides, a moderate amount of independent Gal in its free form was picked up based on the distinctive diagnostic fragments of fully acetylated Gal residues. However, no direct evidence for the explicable mechanism of its existence was obtained. Meanwhile, presence of Glcp-(1→, →4)-Glcp-(1→ and →4,6)-Glcp-(1→ residues, suggested that the LFP-05S fraction was co-extracted with glucan (~10%) composed of a backbone of →4)-D-Glcp-(1→ residues. It should be noted that co-extraction of glucan has been reported in the purification of LFP or other fruit polysaccharides (Zhou et al., 2018; Alba et al., 2020). It persisted in the work up procedures whether as unserviceable individual composition or as synergistic association (self-assembly with the predominant LFP-05S populations for instance) is an interesting future pursuit, but nonetheless it is an indication of the composition of LFP-05S.

3.3. NMR analyses

NMR scalar coupling network assignment was initiated by the isolated reporter clusters of methyl resonances at δ 1.26 and 1.32 ppm (the expansion of TOCSY spectrum embedded in the ^{1}H spectrum in Fig.5A and Fig.5B). This diagnostic pattern was straightforward assigned to H6 of →2)-Rhap-(1→ and →2,4)-Rhap-(1→, respectively. The H6/C6 of →2)-Rhap-(1→ was found at δ 1.26/19.44 and H6/C6 of →2,4)-Rhap-(1→ at δ 1.32/22.89 ppm with the aid of expanded HSQC spectrum embedded in the ^{13}C spectrum (Fig.3C and Fig.3D). COSY and HSQC spectra jointly ascertained the anomeric H/C signals of →2)-Rhap-(1→ at δ 5.29/101.82 ppm. In addition, H5 of →2)-Rhap-(1→ and →2,4)-Rhap-(1→ were determined by the intense H5/H6 correlations at δ 1.26/3.82 and δ 1.32/3.89 ppm in the COSY spectrum. After scanning the TOCSY spectrum where

proton signals belonging to a closed spin system were showcased on a straight line, signals at δ 4.03, 3.73 and 3.42 ppm could be tentatively assigned to H-2, H-3 and H-4 of →2)-Rha$p$-(1→, respectively. The corresponding signals of C2-C5 were further confirmed in the HSQC spectrum. In good accordance with methylation-relied glycosyl linkage analysis, the ratio between →2)-Rha$p$-(1→ and →2,4)-Rha$p$-(1→ was estimated to be 5:1 by integrating the split CH_3 intensities.

Propagation of the magnetization originating from Gal$p$A units strongly preponderated in the spectra. The strong correlation at δ 5.03/100.37 ppm in HSQC was attributed to 1,4-α-D-Gal$p$AOMe. The relevant signals in the COSY and TOCSY spectra individually fixed the position of H2(δ 3.77), H3(δ 3.92), H4(δ 4.45) and H5(δ 4.85), which echoed with the corresponding $^1H/^{13}C$ signals in HSQC spectrum. In good consistence with the glycosidic linkage data, the separated resonances of H5/C5 at δ 4.69-4.85/74.18 ppm in HSQC was a well-suited indicator of methyl esterification in LFP-05S, which had a long-range correlation with COO- at δ178.34 ppm in the HMBC spectrum (Petersen, Meier, Duus, & Clausen, 2008). This was further supported by the presence of a methyl ester signal at δ 4.15/57.89 ppm in the HSQC spectra which coupled with COO- in the HMBC spectrum, indicating the 6-O-methyl esterification of 1,4-α-D-Gal$p$A. Unmethylated free form of 1,4-α-D-Gal$p$A was concomitant on account of ready hydrolysis of the unstable methyl ester, as interpreted by the splitting within the group of H5 signals, supporting a random distribution of free and methyl esterified groups (Grasdalen et al., 1988). Besides, acetate CH_3CO- were observed at δ 1.95, 2.08/30.66 ppm characteristic in HSQC that correlated with COO- at δ184.08 and 177.23 ppm in the HMBC spectrum, respectively, demonstrating that the acetylated resonances were sensitive to the nature of neighboring units. This provided further evidence for identification of →2,4)-Gal$p$A-(1→ and →3,4)-Gal$p$A-(1→ in the methylation analysis, which usually arose from the acetylated characteristic of pectic polymers.

Comprehensive assignment upon the package of NMR spectra facilitated the attributions of characteristic α-Ara-based, β-Gal$p$-based and β-Glc$p$-based residues, designated A through R in Table 2.

Table 2. ^1H and ^{13}C NMR chemical shifts (in ppm) for LFP- 05S (600 MH$_Z$, D_2O, 22 °C)

Peak	Glycosyl residue	H-1/C-1	H-2/C-2	H-3/C-3	H-4/C-4	H-5/C-5	H-6/C-6
A	→2)-α-Rha$p$-(1→	5.29/101.82	4.03/79.45	3.73/72.44	3.42/71.83	3.82/71.25	1.26/19.44

B	→2,4)-α-Rha$p$-(1→	5.27/103.72	4.12/80.60	3.70/69.28	3.83/84.14	3.89/71.44	1.32/22.89
C	α-Gal$p$A-(1→	5.11/101.85	3.79/69.30	3.91/70.02	4.30/73.60	4.41/73.35	174.63
D	→4)-α-Gal$p$A-(1→	5.11/101.85	3.79/69.28	3.92/69.26	4.45/80.57	4.69/73.35	177.70
E	→4)-α-Gal$p$AOMe-(1→	5.03/100.37	3.77/69.28	3.92/69.26	4.45/80.57	4.85/74.18	178.34
F	→3, 4)-α-Gal$p$A-(1→	4.97/101.58	3.59/74.11	3.93/76.39	4.45/80.57	4.69/74.21	181.63
G	→4)-β-Gal$p$A	4.61/99.02	3.52/74.65	3.77 /75.65	4.22/78.89	4.00/73.07	173.81
H	β-Glc$p$-(1→	4.49/106.24	3.28/75.58	3.59/75.82	3.74/77.89	3.72/75.97	3.60,3.97/65.35
I	→4)-β-Glc$p$-(1→	4.53/105.50	3.34/74.63	3.54/78.39	3.87/84.13	3.72/77.90	3.60,3.97/65.35
J	→4,6)-β-Glc$p$-(1→	4.53/105.50	3.34/74.63	3.55/75.87	3.87/84.13	3.72/75.97	3.70/3.92/69.28
K	β-Gal$p$-(1→	4.57/107.75	3.51/74.64	3.55/74.09	3.99/68.73	3.69/77.90	3.78/63.67
L	→3)-β-Gal$p$-(1→	4.70/106.72	3.83/69.08	3.79/75.10	4.23/73.09	3.72/75.97	3.78/63.67
M	→6)-β-Gal$p$-(1→	4.57/107.75	3.48/72.81	3.55/74.09	4.14/73.06	3.92/74.49	3.68,3.80/65.35
N	→3,6)-β-Gal$p$-(1→	4.70/106.72	3.83/69.08	3.79/75.10	4.14/73.06	3.92/74.49	3.68,3.80/65.35
O	α-Ara$f$-(1→	5.10/110.36	4.16//83.80	4.08/77.00	4.14/85.67	3.77/63.80	
P	→3)-α-Ara$f$-(1→	5.24/111.03	4.43/80.58	4.13/84.69	4.14/85.67	3.76/63.80	
Q	→5)-α-Ara$f$-(1→	5.25/112.06	4.26/84.15	3.98/79.39	4.14/85.67	3.67, 3.80/65.26	
R	→3,5)-α-Ara$f$-(1→	5.25/112.06	4.41/86.72	4.07/82.72	4.09/84.12	3.67, 3.80/65.26	

To complete the description of the structure, the connectivity paths between adjacent glycosyl residue cycles and position of appended groups were defined by the heteronuclear coupling of ^{1}H-^{1}H in NOESY as well as ^{1}H-^{13}C in HMBC correlation maps, respectively. Further, the contact between H1 of 1, 2-α-Rha$p$ [or 1,2,4-α-Rha$p$, hereafter] and H-4 of 1,4-α-D-Gal$p$A [or 1,4-α-Gal$p$A-OMe, hereafter] was easily identified using the strong NOE correlation at δ 5.27/4.45 ppm. In addition, an intra-contact between H1 and H5 of 1, 2-α-Rha$p$, along with inter-contacts between H1 of 1, 2-α-Rha$p$ and H-1 as well as H3 and H5 of 1,4-α-Gal$p$A, led to the linkage pattern identification of 1, 2-α-Rha$p$ to the O-4 position of 1,4-α-Gal$p$A. This was further confirmed by the H1 of 1, 2-α-Rha$p$ /C4 of 1,4-α-Gal$p$A correlation at δ 5.27/ 80.57 ppm in HMBC.

Following the identical approach, the linkage of 1,4-α-D-Gal$p$A to the O-2 position of 1, 2-α-Rha$p$ was determined using the through-space coupling profile. Upon these mutually reflective correlation, the repeated units were established as interspersed [→ 2)-α-Rha$p$-(1→4)-α-Gal$p$A-

(1→2)-α-Rha*p*-(1→], which was typically present in the RG-I moieties of acidic heteropolysaccharides.

The 1,4-α-Gal*p*A was linked to an adjacent 1,4-α-Gal*p*A or 1,4-α-Gal*p*A-OMe residue as indicated by the inter-residual cross contact of H1 to H4 at δ 5.11/4.45 and δ 5.05/4.45 ppm as well as H4 to H1 at δ 4.45/5.05 ppm in NOESY. Furthermore, the correlation between δ 5.11/4.45 ppm also pointed to the linkage of H1 of terminal α-Gal*p*A to the adjacent 1,4-α-Gal*p*A. H1/H2, H1/H3, and H3/H4 arose from the intra-residual cross contact of 1,4-α-Gal*p*A at δ 5.11/3.79, 5.11/3.92, and 3.92/4.45 ppm, respectively, along with inter-residue contact between the H2 of 1,4-α-Gal*p*A-OMe and H4 of 1,4-α-Gal*p*A at δ 3.77/4.45 ppm, H1 to C4 at δ 5.11/80.57 ppm and H4 to C1 at δ 4.45/101.85 ppm, and this hence confirmed the establishment of HG moiety in LFP-05S.
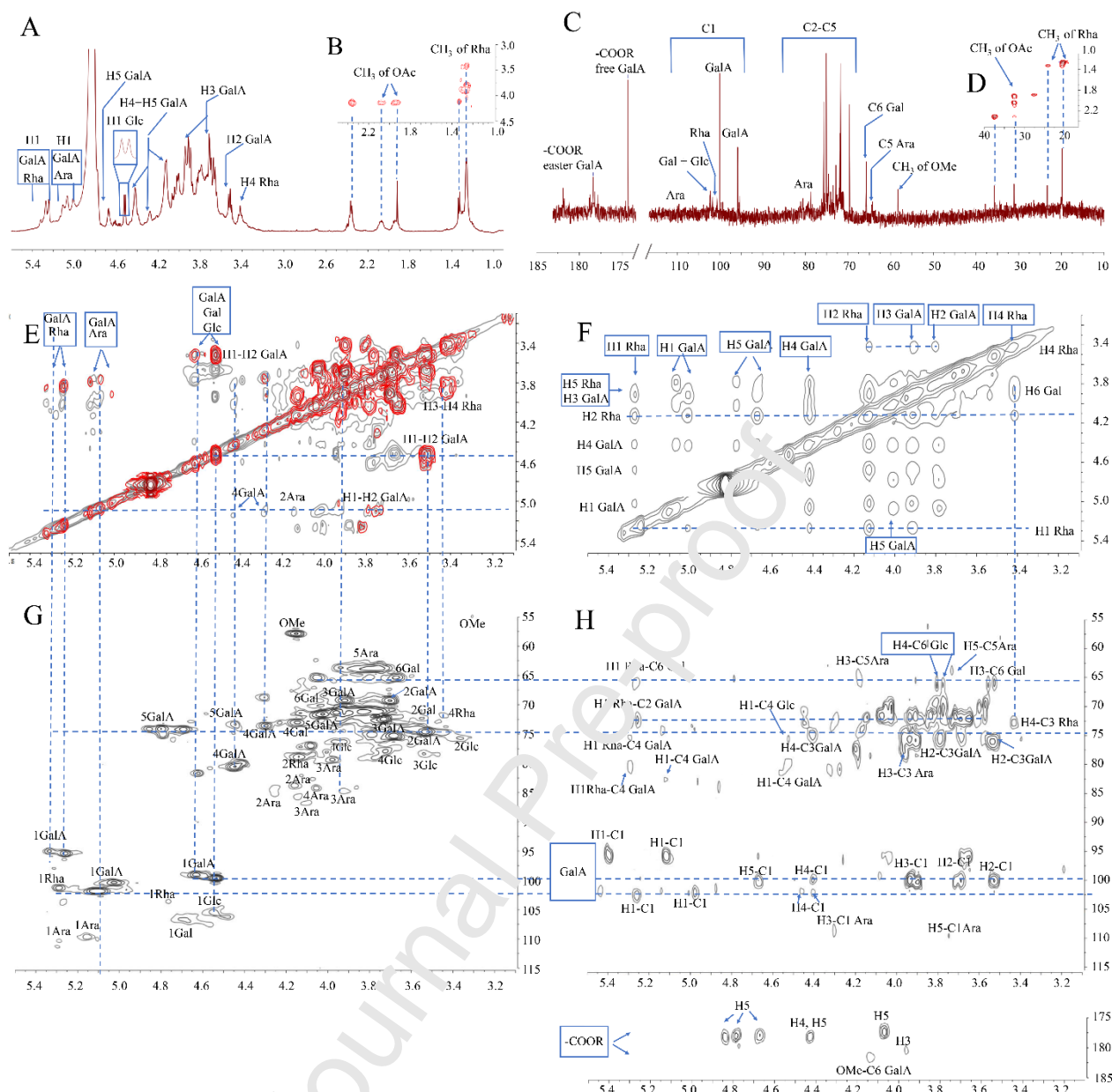
Fig. 3. NMR spectra recorded for LFP-05S (600 MHz, 22°C, in 20 mM NaOD): (A) ^{1}H NMR spectrum with (B) selected region of TOCSY spectrum; (C) ^{13}C NMR spectrum with (D) selected region of HSQC spectrum; (E) superimposed COSY (red) and TOCSY spectrum(grey) where the massive crisscross peaks of D$_2$O at δ 4.83/ 4.83 ppm were artificially covered to avoid interference; (F) NOESY spectrum; (G) HSQC and (H) HMBC spectrum. Correlations of special peaks within and between spectra were connected with blue dotted line.

Other correlations of the densities were inferred through the same formalism as denoted in Fig.3, which led to the modular organizational structure of arabinogalactan and arabinan located at

the O-4 position of →2,4)-Rha*p*-(1→ as side chains of RG-I. Generally, it was evident that the NMR substantiated the structural information about the linkages within the connecting residues identified through methylation.

The structural similarity of the constituent units caused signal convergence in the carbinolic region and hence hindered any possibility to proceed further disentanglement of micro-heterogeneity in LFP-05S. Univocal characterization to tackle the existing gaps will be addressed in future depending on the emergence of unbiased and unambiguous approaches beyond the as of yet empirical assignment. The cumulative interconnected arrangement allowed tentative establishment of the schematic structure in Fig. 4, wherein the stretches of fairly long linier HG backbone were covalently flanked by alternating sequences of intra-RG-I linkers. The neutral AG and arabinan organized the bushy sidechains at C-4 of Rha*p* along the backbone axis and hence forming the twisted "hairy regions".
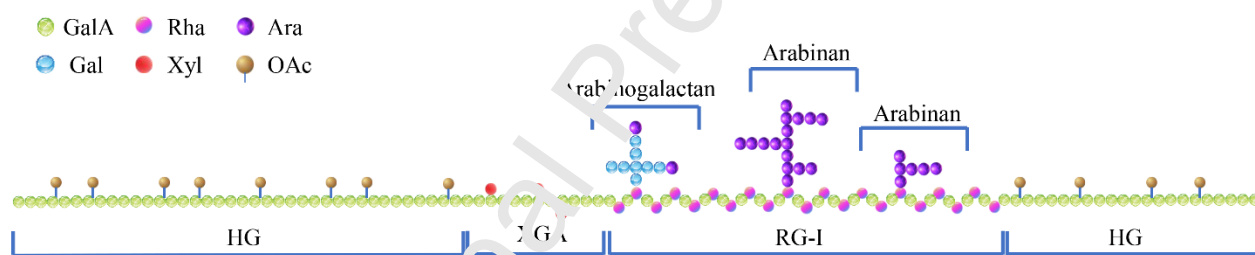

Fig.4. Schematic primary structure model of LFP-05S backbone with branched side chains

Acidic polysaccharides with similar structural blocks were reported in recent literature from different plant resources across unicellular algae (Palacio-Lopez et al., 2020), gymnosperms (Mohnen, 2008) and angiosperms (Noguchi et al., 2020). The highly conservative structure and composition, with HG and RG-I representing the most abundant forms decorated with neutral side chains, provided convincing basis as to the significance this cellular component has displayed in cell development, differentiation, morphogenesis, inter- and intra-cellular communication and environmental sensing in the evolutionary history (Shin, et al, 2021). On the other side, despite the similarity of the constituent elements, diverse LFPs are emerging in recent literature with substantial variation in structural organization and complexity, from linear →4)-α-GalA-(1→ to highly branched arabinogalactan backbone substituted with versatile sidechains (Masci et al., 2018). LFP-05 was not identical with reported polysaccharides with regard to the microcosmic chemical

architecture. The unsurprising difference might originate from the innate structural complexity in the dynamic wall infrastructure, the internal genetic variability of the *L. fructus* cultivars, or the adaptive response of *Lycium barbarum* L. to the external ecosystem. The application of different processing, extraction, and selective purification employed may also have considerable influence on the structural variations (Yi et al., 2020). The differentiated structures opened new windows for future investigations into the distribution of structurally diversified LFPs and structure-activity relationship.

3.4. Defensive modulation of LFP-05S against PQ-induced damage in oxidative stress model worms

Microscopic nematode *C.elegans* has emerged as an advantageous *in vivo* non-rodent model organism for mechanism interpretation and high-throughput candidate drug screenings ranging from aging, toxicity, and related disorders or diseases (Maglioni, Arsalan, & Ventura, 2016). Therefore, to provide direct evidence for its potential application in aging or related disorders, the current study intended to dissect the modulation of LFP-05S in both oxidative stress and standard conditions upon survival and phenotypic effect in *C. elegans*.
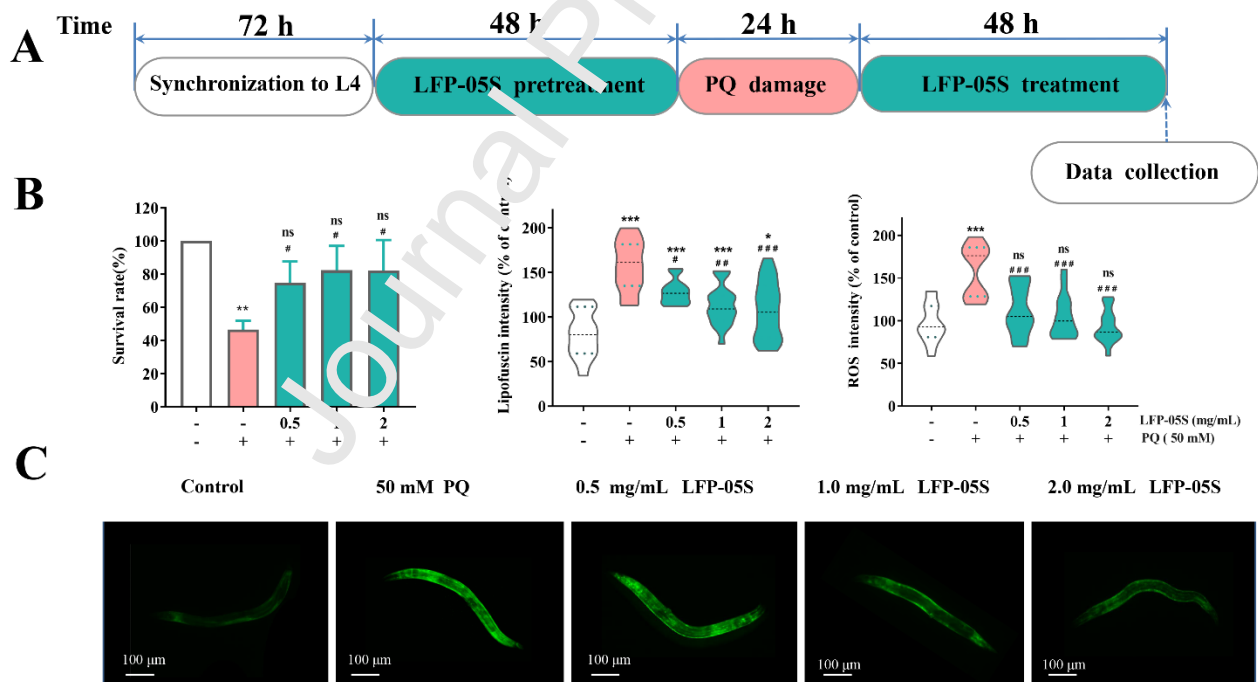

Fig.5. Defensive role of LFP-05S against oxidative stress in PQ-challenged worms: (A) Schematic diagram of experimental design; (B) Effect of LFP-05S on worm survival, lipofuscin intensity and ROS production in PQ-insulted worms; (C) Representative fluorescence micrograph for lipofuscin accumulation. Data presented as mean (n=3) ± SEM of three independent experiments (* $p < 0.05$,

** $p < 0.01$, *** $p < 0.001$ as compared with control worms, [#] $p < 0.05$, [##] $p < 0.01$, [###] $p < 0.001$ as compared with PQ-challenged worms, and ns: no significance, hereafter).

The L4 worms sorted by age were subjected to addition of LFP-05S and/or damaged by strong redox cycler PQ to model sensitivity and response to oxidative damage following the timeline shown in Fig.5A. The survival was remarkably compromised by PQ insult as compared with the untreated counterpart. Nevertheless, feeding with LFP-05S progressively rescued the decreased survival in a dose-dependent manner (Fig. 5B).

Lipofuscin granules are the end-product of lipid peroxidation that accumulates during aging process and oxidative stress and they hence, represent a promising aging marker. The LFP-05S feeding reinforced the clearance of lipofuscin (Fig.5B and 5C), indicating that LFP-05S gradually obliterated the occurrence of PQ-induced accelerated lipofuscin accumulation. Furthermore, continuous feeding of LFP-05S progressively decreased the untoward overproduction of ROS after 48 hours of recovery from PQ insult. This pattern of worm survival, lipofuscin accumulation, and ROS production ambiguously demonstrated that exogenous LFP-05S counteracted the PQ-triggered oxidative stress and also conferred defensive roles against PQ impairment in *C. elegans*.

3.5. LFP-05S improved the antioxidant defense system under PQ-induced oxidative stress scenario

Redox homeostasis is crucial for the stable maintenance of normal physiology. High level of oxidative stress may initiate undesired injury when stockpile of oxidation products is overloaded to the systematic adaptation. Given the ROS production was positively modulated by LFP-05S supplement under the oxidative stress scenario, the indices interpreting oxidative stress were tracked to further assess the defensive activity of LFP-05S against etiologic oxidative stress.
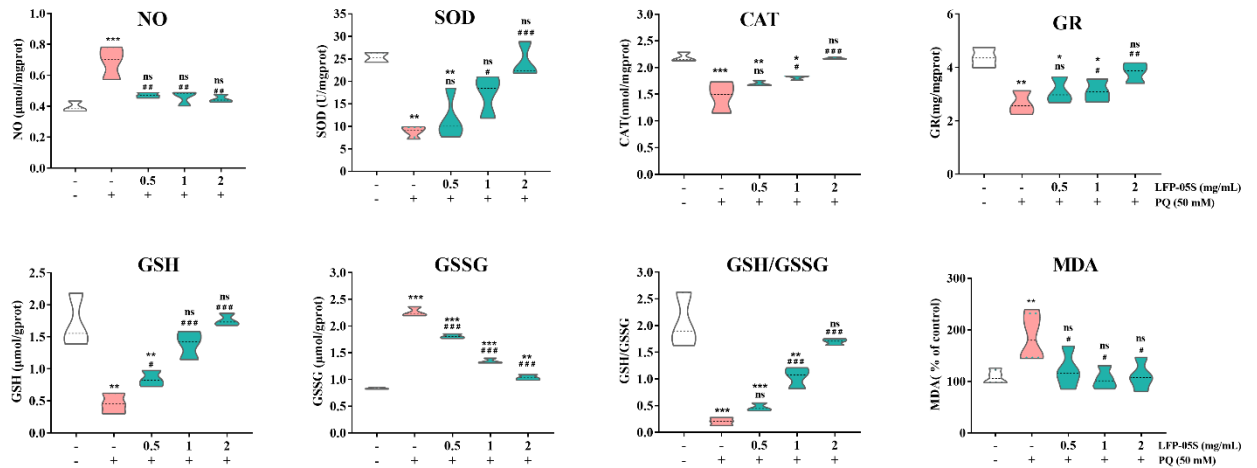
Fig.6. LFP-05S mitigated PQ-induced oxidative stress scenario in N2 worms (NO production, anti-oxidant enzyme activities of SOD, CAT and GR, GSH content, GSSG content, GSH/GSSG and MDA level)

The targets of the oxidative stress triggered by PQ were heterogeneously complicated which involved disorganization of the antioxidant system. The level of NO was increased in line with the ROS production by imposed PQ stimulus as compared with the basal level in physiological redox state. As part of an adaptive response, the outweighed NO, the weakened enzymic (SOD, CAT and GR activities) and non-enzymic (GSH level and GSH/GSSG) defense system, collectively suggested that the detrimental disequilibration between internal reduction and oxidation was initiated by PQ. Consequently, elimination of xenobiotics metabolites was hence impaired and this was manifested through the elevated formation of MDA which was the downstream end products of lipid peroxidation (Fig.6). On top of this disequilibration, the massive oxidative stress was obviously ameliorated through intervention of LFP-05S. The overproduction of NO was terminated, and was accompanied by the emergence of the reactivated endogenous enzymic and non-enzymic defensing. Expectedly, the renewed anti-oxidative network enhanced the lipid peroxidation indicated by the drop of MDA level. These events pointed to the suggestion that exogenous LFP-05S feeding was able to be compensated for the adverse consequences of the oxidative stress-associated physiological characteristics by reversing the disturbed state of endogenous anti-oxidants defense barriers.

3.6. LFP-05S prolonged longevity without propagation impairment of C. elegans under normal cultivate conditions

Enhanced capacity of dealing with oxidative stress has been proved to be mechanistically associated with extension of lifespan in *C. elegans,* and thus rendering the stress tolerance a determinant of longevity (Urban et al., 2017). After the evaluation of LFP-05S on oxidative stress subjected to forced oxidative stimuli, addressed was the issue of whether LFP-05S would also exhibit positive potency on the longevity or senescence delay under normal conditions.
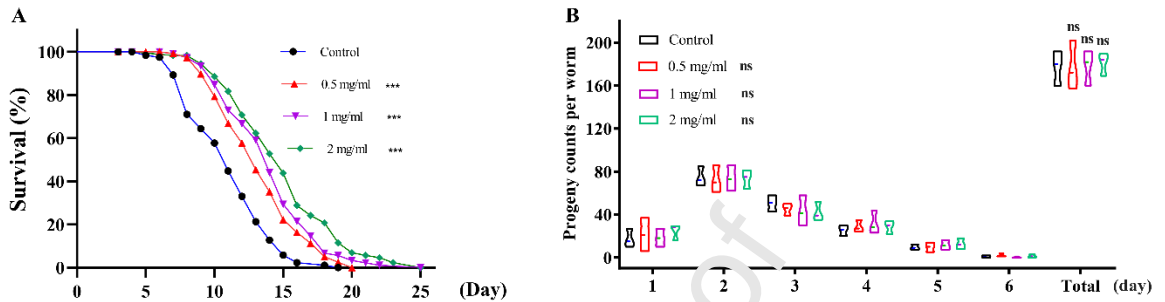

Fig.7. LFP-05S elongated lifespan under standard conditions at 20°C in N_2 worms. (A) The Kaplan-Meier survivorship curves depicting the effect of LFP-05S on the lifespan of N_2 worms cultured on standard conditions. Combined data of four independent biological trials were presented. (B) Progeny production per day and the total count per worm during the adult stage of reproduction.

Input of LFP-05S expectedly elicited significant concentration-dependent extension in overall lifespan of *C. elegans* wherein, 2 mg/ml LFP-05S feeding extended the mean and maximum lifespan by up to 25.70 and 18.50% respectively (Fig.7A). Notably, it was found that the offspring counts at all the tested concentrations underwent similar patterns which showed a sharp increase in day 2 followed by gradual decline till the endpoint of the reproduction assay. However, it was noted that neither the daily nor the total number of descendants showed statistical significance compared with control and this indicted negligible impact of LFP-05S on propagation of *C. elegans* (Fig. 7B).

The results were correlated with previous reports supporting that stress resistance and life span are usually connected. Despite the above hint on the observed beneficial effects, the exact molecular basis requires further elucidation. LFP-05S-suppliment did not statistically affected the offspring counts as compared to the vehicle control, suggesting that LFP-05S might act independent of a dietary restriction-like mechanism (Mohankumar et al., 2020). Through literature review, the signaling pathways of anti-oxidant regulation and longevity, including the Nrf2/SKN-1, SIRT1/SIR 2.1, and FOXO/DAF-16 pathways, might be involved in the phenotype conferred by LFP-05S (González-Peña, Lozada-Ramírez, & Ortega-Regules, 2021; Duangjan, Rangsinth, Gu, Wink, & Tencomnao, 2019; Wang et al., 2021). Future studies should unravel the molecular details of

process steps required for the antioxidant response occur that enable LFP-05S to protect from oxidative insult and to extend lifespan.

4. Conclusions

In conclusion, the present work unveiled the macromolecular architecture and the potential for alleviation of oxidative stress and senescence delay of an acidic heteropolysaccharide, LFP-05S, purified from *L. fructus*. The dominant of LFP-05S was a highly heterogeneous population comprised of distinct linear HG and RG-I-type backbone, with topological neutral arabinan and arabinogalactan domains branched at O-4 of the →2)-Rha*p*-(1→ residues. The net impact of exogenous LFP-05S on the aging process was evaluated based on the changes in PQ-damaged oxidative stress models and normal physiologic *C. elegans*. LFP-05S successfully compensated the adverse consequences of PQ. In detail, LFP-05S was capable of reducing the intracellular ROS levels and exhibited defensive modulation by strengthening both the enzymic and non-enzymic defense systems, indicating that regeneration of the endogenous redox status may encode the underlying mechanism contributing to the protective power of LFP-05S during deleterious oxidative stress.

The protective features, paralleled with LFP-05S's positive potency on the longevity of *C. elegans* under normal conditions, endorsed the pharmacological basis for the starting hypothesis of LFP's antioxidative activity and its potential use in aging scenarios where oxidative stress are the key players. Nevertheless, a number of critical questions remain open. One concerns the elucidation of structural heterogeneity. The structural framework of LFP-05S was currently put forward as exclusive polysaccharide, ignoring the invariably contained but significant non-saccharide glycoconjugates, which may in essence gain access to polysaccharide compartments through undiscovered mechanisms (Flynn *et al.,* 2021). The structural characterization was incomplete and pointed to a new axis of clues if and how the expanded templates mediate in the architecture of LFP-05S. Another formidable challenge lies within deciphering the unequivocal molecular basis of the beneficial response LFP-05S elicited given the complexity of the hallmarks and regulators in longevity pathways that are being uncovered. There is need for much additional work upon both *C. elegans* and higher model organisms to yield additional validations and full understanding for the proof-of-concept. Despite the interpretative constraints, the efforts of the current work highlighted the application feasibility of LFP-05S in terms of developing a practically therapeutic intervention, or at least an alternative to counteract aging and oxidative stress-associated declines.

Author Contributions: Conceptualization, J-A. D, F. Z, and X. Z; Data Curation, F. Z, X. Z, X. L, K. W, Y. C, T. M, S. G, P. C, S. Y, Q. R, C. X and C. L; Formal Analysis, F. Z, X. Z, X. L, K. W

Conflict of interest: None.

References

Agrawal, P. K. (1992). NMR Spectroscopy in the structural elucidation of oligosaccharides and glycosides. *Phytochemistry*, *31*(10), 3307–3330.

Alba, K., Offiah, V., Laws, A. P., Falade, K. O., & Kontogiorgos, V. (2020). Baobab polysaccharides from fruits and leaves. *Food Hydrocolloids*, *106*, 105874.

Ben, M., Haddar, A., Ghazala, I., Ben, K., & Brisset, C. (2017). Optimization of polysaccharides extraction from watermelon rinds : Structure , functional and biological activities. *Food Chemistry*, *216*, 355–364.

Dall, K. B., & Færgeman, N. J. (2019). Metabolic regulation of lifespan from a C . elegans perspective, *Gene & Nutrition, 14,* 25.

Duangjan, C., Rangsinth, P., Gu, X., Wink, M., & Tencomnao, T. (2019). Lifespan extending and oxidative stress resistance properties of a leaf extracts from anacardium occidentale L. in caenorhabditis elegans. *Oxidative Medicine and Cellular Longevity*, *2019*, 9012396.

Eder, S., Zueblin, P., Diener, M., Peydayesh, M., Boulos, S., Mezzenga, R., & Nyström, L. (2021). Effect of Polysaccharide Conformation on Ultrafiltration Separation Performance. *Carbohydrate Polymers*, *260*, 117830.

Flynn, R. A., Pedram, K., Malaker, S. A., Batista, P. J., Smith, B. A. H., Johnson, A. G., … Bertozzi, C. R. (2021). Small RNAs are modified with N-glycans and displayed on the surface

of living cells. *Cell*, *184*, 3109-3124.

González-Peña, M. A., Lozada-Ramírez, J. D., & Ortega-Regules, A. E. (2021). Carotenoids from
mamey (Pouteria sapota) and carrot (Daucus carota) increase the oxidative stress resistance of
Caenorhabditis elegans. *Biochemistry and Biophysics Reports*, *26,* 100989.

Goya, M. E., Xue, F., Sampedro-Torres-Quevedo, C., Arnaouteli, S., Riquelme-Dominguez, L.,
Romanowski, A., … Doitsidou, M. (2020). Probiotic Bacillus subtilis Protects against α-
Synuclein Aggregation in C. elegans. *Cell Reports*, *30*(2), 367-380.

Grasdalen, H., Einar Bakøy, O., & Larsen, B. (1988). Determination of the degree of esterification
and the distribution of methylated and free carboxyl groups in pectins by 1H-n.m.r.
spectroscopy. *Carbohydrate Research*, *184*, 183–191.

Hart, G., W. & Copeland, R., J. (2010). Glycomics Hits the Big Time. *Cell, 143(5)*, 672–676.

Lehrfeld, J. (1987). Simultaneous gas-liquid chromatographic determination of aldoses and
alduronic acids. *Journal of Chromatography A*, *408*, 245–253.

Luo, J., Mills, K., le Cessie, S., Noordam, R., van Heemst, D. (2020). Ageing, age-related diseases
and oxidative stress: What to do next? Ageing Research Reviews, 57, 100982.

Maglioni, S., Arsalan, N., & Ventura, N. (2016). C. elegans screening strategies to identify pro-
longevity interventions. *Mechanisms of Ageing and Development*, *157*, 60–69.

Masci, A., Carradori, S., Casadei, M. A., Paolicelli, P., Petralito, S., Ragno, R., & Cesa, S. (2018).
Lycium barbarum polysaccharides: Extraction, purification, structural characterisation and
evidence about hypoglycaemic and hypolipidaemic effects. A review. *Food Chemistry*, *254*,
377–389.

Meng J., Lv Z., Guo M., Sun C., Li X., Jiang Z., A … Chen C. (2022) Lycium barbarum extract
inhibits β-amyloid toxicity by activating the antioxidant system and mtUPR in a
Caenorhabditis elegans model of Alzheimer's disease. *The FASEB Journal*, *36*(2):e22156.

Meng, J., Lv, Z., Sun, C., Qiao, X., & Chen, C. (2020). An extract of Lycium barbarum mimics

exercise to improve muscle endurance through increasing type IIa oxidative muscle fibers by activating ERRγ. *FASEB Journal*, *34*(9), 11460–11473.

Mohankumar, A., Kalaiselvi, D., Thiruppathi, D., Muthusaravanan, S., Nivitha, S., Levenson, C ...Sundararaj, P. (2020) α-and β-Santalols Delay Aging in Caenorhabditis elegans via Preventing Oxidative Stress and Protein Aggregation. *ACS Omega*, 5(50): 32641-32654.

Mohnen, D. (2008). Pectin structure and biosynthesis. *Current Opinion in Plant Biology*, *11*(3), 266–277.

Nguyen, T. A., Do, T. T., Nguyen, T. D., Pham, L. D., & Nguyen, V. Du. (2011). Isolation and characteristics of polysaccharide from Amorphophallus corrugatus in Vietnam. *Carbohydrate Polymers*, *84*, 64–68.

Noguchi, M., Hasegawa, Y., Suzuki, S., Nakazawa, M., Ueda, M., & Sakamoto, T. (2020). Determination of chemical structure of pea pectin by using pectinolytic enzymes. *Carbohydrate Polymers*, *231*, 115738.

Oliveira, A. F. De, Erdmann, G., Iacomini, M., Mach, L., Cordeiro, C., & Cipriani, T. R. (2017). Chemical structure and anti-inflammatory effect of polysaccharides obtained from infusion of Sedum dendroideum leaves. *International Journal of Biological Macromolecules*, *105*, 940–946.

Palacio-Lopez, K., Sun, L., Reed, R., Kang, E., Sørensen, I., Rose, J. K. C., & Domozych, D. S. (2020). Experimental Manipulation of Pectin Architecture in the Cell Wall of the Unicellular Charophyte, Penium Margaritaceum. *Frontiers in Plant Science*, *11*, 1–22.

Petersen, B. O., Meier, S., Duus, J., & Clausen, M. H. (2008). Structural characterization of homogalacturonan by NMR spectroscopy-assignment of reference compounds. *Carbohydrate Research*, *343*, 2830–2833.

Pettolino, F. A., Walsh, C., Fincher, G. B., & Bacic, A. (2012). Determining the polysaccharide composition of plant cell walls. *Nature Protocols*, *7*(9), 1590–1607.

Poljsak,B., Šuput, D. and Milisav.I. (2013). Achieving the balance between ROS and antioxidants:

When to use the synthetic antioxidants. *Oxidative Medicine and Cellular Longevity*, *2013*, 956792.

Redgwell, R. J., Curti, D., Wang, J., Dobruchowska, J. M., Gerwig, G. J., Kamerling, J. P., & Bucheli, P. (2011). Cell wall polysaccharides of Chinese Wolfberry (Lycium barbarum): Part 2 . Characterisation of arabinogalactan-proteins. *Carbohydrate Polymers*, *84*, 1075–1083.

Santos, M. A., Franco, F. N., Caldeira, C. A., de Araujo, G. R., Vieira, A., … Lara, R. C. (2021). Antioxidant effect of Resveratrol: Change in MAPK cell signaling pathway during the aging process. *Archives of Gerontology and Geriatrics, 92*, 104266.

Shin,Y., Chane, A., Jung, M., and Lee, Y. (2021). Recent Advances in Understanding the Roles of Pectin as an Active Participant in Plant Signaling Networks. *Plants, 10,* 1712.

Sims, I. M., Carnachan, S. M., Bell, T. J., & Hinkley, S. F. R. (2018). Methylation analysis of polysaccharides : Technical advice. *Carbohydrate Polymers, 188*, 1–7.

Sindhu, R. K., Goyal, A., Das, J., Neha, Choden, S., & Kumar, P. (2021). Immunomodulatory potential of polysaccharides derived from plants and microbes: A narrative review. *Carbohydrate Polymer Technologies and Applications*, *2*, 100044.

Urban, N., Tsitsipatis, D., Hausig, F., Kreuzer, K., Erler, K., Stein, V., … Klotz, L. O. (2017). Non-linear impact of glutathione depletion on C. elegans life span and stress resistance. *Redox Biology*, *11*, 502–515.

Wang, H., Zhang, S., Zhai, L., Sun, L., Zhao, D., Wang, Z., & Li, X. (2021). Ginsenoside extract from ginseng extends lifespan and health span in Caenorhabditis elegans . *Food & Function*, 12, 6793-6808.

Xiao, Z., Deng, Q., Zhou, W., & Zhang, Y. (2022). Immune activities of polysaccharides isolated from Lycium barbarum L. What do we know so far? *Pharmacology and Therapeutics*, *229*, 107921.

Yi, Y., Xua, W., Wang, H., Huang, F., Wang, L. (2020). Natural polysaccharides experience

physiochemical and functional changes during preparation: A review. *Carbohydrate Polymers, 234,* 115896.

Yokoyama, R. (2020). A Genomic Perspective on the Evolutionary Diversity. *Plants, 9,* 1195.

Yu, D. H., Wu, J. M., & Niu, A. J. (2009). Health-promoting effect of LBP and healthy Qigong exercise on physiological functions in old subjects. *Carbohydrate Polymers*, *75*, 312–316.

Zhang, F., Zhang, X., Guo, S., Cao, F., Zhang, X., Wang, Y., … Duan, J. ao. (2020). An acidic heteropolysaccharide from Lycii fructus: Purification, characterization, neurotrophic and neuroprotective activities in vitro. *Carbohydrate Polymers*, *245*, 116894.

Zhang, Z., Zhou, Y., Fan, H., Billy, K. J., Zhao, Y., Zhan, X., … Ba, Y. (2019). Effects of Lycium barbarum Polysaccharides on Health and Aging of C. elegans Depend on daf-12/daf-16 . *Oxidative Medicine and Cellular Longevity*, *2019*, 6379493.

Zhou, L., Liao,W., Chen, X., Yue,H., Li,H., Ding,K. (2018). An arabinogalactan from fruits of Lycium barbarum L. inhibits production and aggregation of Aβ42. Carbohydrate Polymers, 195, 643-651.

Zhou, L., Liao, W., Zeng, H., Yao, Y., Chen, X., & Ding, K. (2018). A pectin from fruits of Lycium barbarum L. decreases β-amyloid peptide production through modulating APP processing. *Carbohydrate Polymers*, *201*, 65–74.
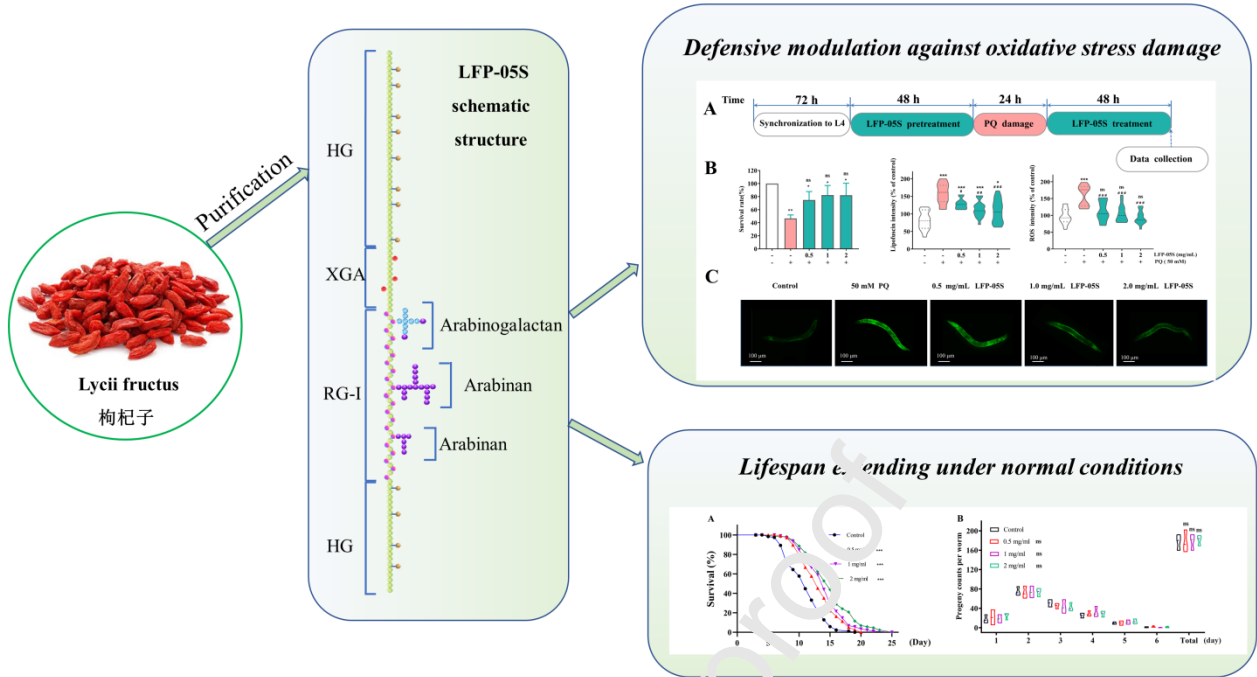
Declaration of interests

☒ The authors declare that they have no known competing financial interests or personal relationships that could have appeared to influence the work reported in this paper.

☐The authors declare the following financial interests/personal relationships which may be considered as potential competing interests:

Graphical abstract

Highlights

1. An acidic polysaccharide (LFP-05S) was purified from Lycii fructus.

2. Homogalacturonan domain dominated in LFP-05S.

3. LFP-05S exhibited defensive modulation in paraquat-damaged oxidative stress *Caenorhabditis elegans*.

4. LFP-05S extended lifespan of *Caenorhabditis elegans* under normal conditions.